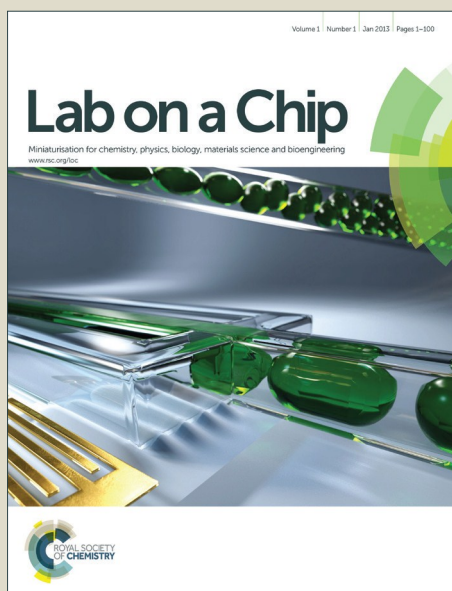


Lab on a Chip

Accepted Manuscript



This is an *Accepted Manuscript*, which has been through the Royal Society of Chemistry peer review process and has been accepted for publication.

Accepted Manuscripts are published online shortly after acceptance, before technical editing, formatting and proof reading. Using this free service, authors can make their results available to the community, in citable form, before we publish the edited article. We will replace this *Accepted Manuscript* with the edited and formatted *Advance Article* as soon as it is available.

You can find more information about *Accepted Manuscripts* in the [Information for Authors](#).

Please note that technical editing may introduce minor changes to the text and/or graphics, which may alter content. The journal's standard [Terms & Conditions](#) and the [Ethical guidelines](#) still apply. In no event shall the Royal Society of Chemistry be held responsible for any errors or omissions in this *Accepted Manuscript* or any consequences arising from the use of any information it contains.

1 Deformability based Sorting of Red Blood Cells Improves Diagnostic Sensitivity 2 for Malaria Caused by Plasmodium Falciparum

3 Quan Guo^a, Simon P. Duffy^a, Kerryn Matthews^a, Xiaoyan Deng^a, Aline T. Santoso^a, Emel Islamzada^a and
4 Hongshen Ma^{a,b,c}

5 *a Department of Mechanical Engineering, University of British Columbia, 2054-6250 Applied Science Lane,*
6 *Vancouver, BC, Canada V6T 1Z4*

7 *b Department of Urologic Science, University of British Columbia, Vancouver, BC, Canada*

8 *c Vancouver Prostate Centre, Vancouver General Hospital, Vancouver, BC, Canada*

9

10 **ABSTRACT**

11 The loss of red blood cell (RBC) deformability is part of the pathology of many diseases. In malaria
12 caused by *Plasmodium falciparum* infection, metabolism of hemoglobin by the parasite results in
13 progressive reduction in RBC deformability that is directly correlated with the growth and development
14 of the parasite. The ability to sort RBCs based on deformability therefore provides a means to isolate
15 pathological cells and to study biochemical events associated with disease progression. Existing methods
16 have not been able to sort RBCs based on deformability or to effectively enrich for *P. falciparum*
17 infected RBCs at clinically relevant concentrations. Here, we develop a method to sort RBCs based on
18 deformability and demonstrate the ability to enrich the concentration of ring-stage *P. falciparum*
19 infected RBCs (*Pf*-iRBCs) by >100X from clinically relevant parasitemia (<0.01%). Deformability based
20 sorting of RBCs is accomplished using ratchet transport through asymmetrical constrictions using
21 oscillatory flow. This mechanism provides dramatically improved selectivity over previous biophysical
22 methods by preventing the accumulation of cells in the filter microstructure to ensure that consistent
23 filtration forces are applied to each cell. We show that our approach dramatically improves the
24 sensitivity of malaria diagnosis performed using both microscopy and rapid diagnostic test by converting
25 samples with difficult-to-detect parasitemia (<0.01%) into samples with easily detectable parasitemia
26 (>0.1%).

27 **ONE SENTENCE SUMMARY**

28 Sorting red blood cell based on deformability improves sensitivity of malaria diagnosis by >100X.

29 **KEY WORDS**

30 Red blood cells, Cell sorting, Deformability, *Plasmodium falciparum*, Malaria, Diagnosis
31
32
33

Deformability based sorting of red blood cells

34 **INTRODUCTION**

35 The ability to extensively and repeatedly deform is essential to the function of red blood cells (RBCs)
36 as they transport oxygen and carbon dioxide throughout the body. The loss of this capability can
37 contribute to microvascular occlusions resulting in tissue necrosis and organ failure, as observed in
38 malaria^{1,2}, sickle cell disease³, and thalassemia⁴. The loss of RBC deformability is particularly important in
39 malaria because the parasite metabolizes hemoglobin into the toxic by-product, heme, which induces
40 stiffening of the cell membrane through lipid peroxidation and cytoskeleton cross-linking⁵. Given the
41 critical importance of RBC deformability, sorting cells based on this parameter provides a means to
42 separate pathological cells from normal cells to improve diagnostic sensitivity, as well as to elucidate
43 molecular processes associated pathogenesis.

44 Existing benchtop approaches for sorting RBCs include density gradient centrifugation⁶ and flow
45 cytometry^{7,8}. The former has limited selectivity while the latter involves DNA fluorescent labeling that is
46 often confounded by leukocyte and reticulocyte contamination, as well as auto-fluorescence and RNA
47 non-specific staining⁸. RBCs have been biophysically separated based on size, deformability,
48 permeability and cyto-adherence, using deterministic lateral displacement^{9,10}, margination^{11,12},
49 dielectrophoresis¹³, and surface-enhanced cyto-adherence¹⁴. These methods are effective when there
50 are significant differences between target and background cells, such as for *Plasmodium falciparum*
51 infected RBCs (*Pf*-iRBCs) at late (trophozoite and schizont) stages of infection. However, these methods
52 are not effective when target cells are distinguished by more subtle differences, such as for *Pf*-iRBCs at
53 the ring stage of infection, which is typically what's found in clinical blood samples^{15,16}. *Pf*-iRBCs can also
54 be isolated using magnetic attraction of biocrystallized hemozoin. This approach is very effective for
55 isolating late stage *Pf*-iRBCs¹⁷ and recently been shown to have some effect on early stage *Pf*-iRBCs,
56 although only at high parasitemia¹⁸. None of the existing approaches, however, provide an effective
57 method to sort RBCs based on deformability, as well as to enrich for early stage *Pf*-iRBCs at clinically
58 relevant concentrations (<0.01%).

59 Micropore filtration has long been considered as a method to sort cells based on deformability. This
60 approach has been used successfully to separate cancer cells from leukocytes¹⁹⁻²², as well as nucleated
61 cells from RBCs^{23,24}, but has not been able to sort ultra-soft cells like RBCs. This lack of selectivity for
62 sorting RBCs arises from the inability to precisely control the pressure applied to each cell during the
63 sorting process. In a standard membrane filter, the force used to deform each cell is determined by the
64 pressure difference across the filtration microstructures, which is dictated by the sample flow rate and

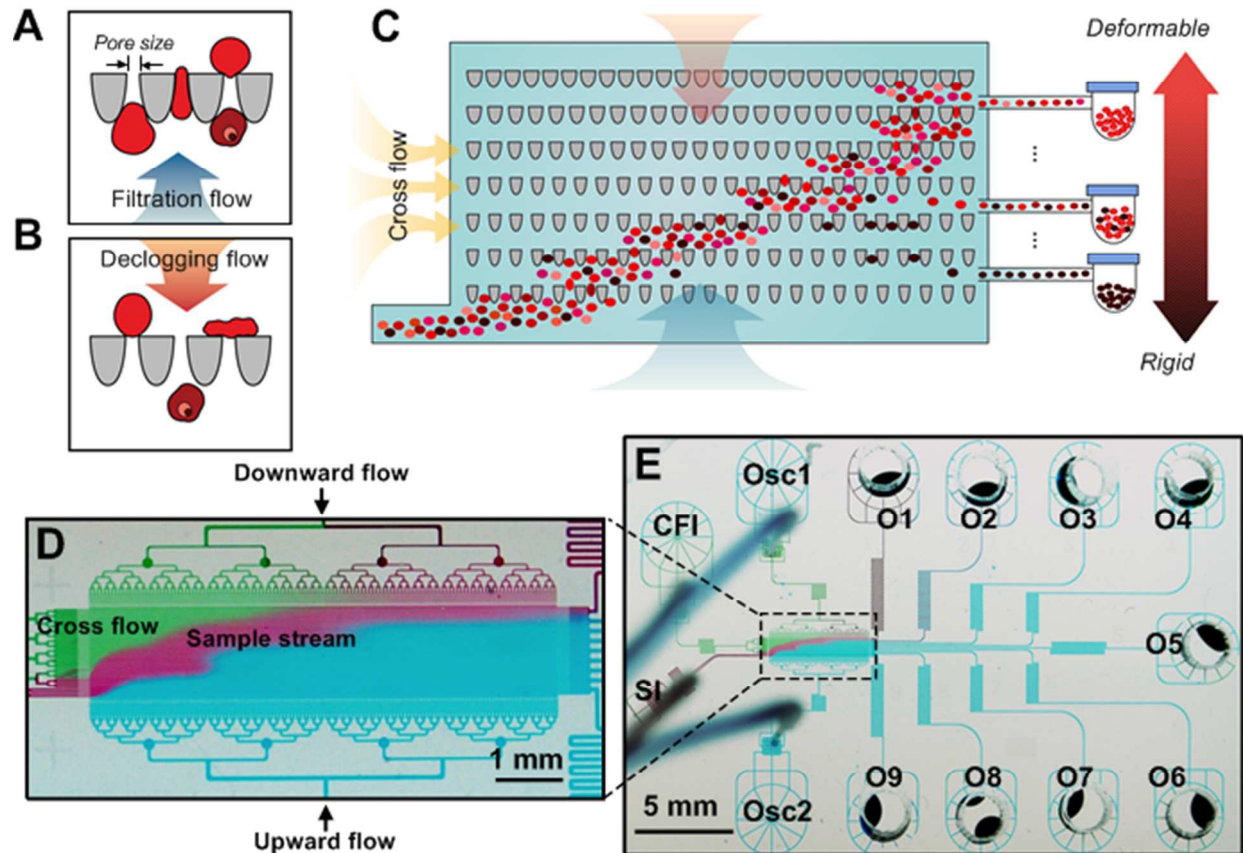
Deformability based sorting of red blood cells

65 the hydrodynamic resistance of the filtration microstructure. As cells are captured in the filter
66 microstructure, its hydrodynamic resistance increases in an unpredictable manner, significantly varying
67 the filtration force applied to each cell. Additionally, prolonged contact between the cells and the
68 filtration microstructures promotes adsorption, making it generally impossible to extract captured cells
69 after separation. This problem is further exaggerated for *Pf*-iRBCs, which exhibit increased cyto-
70 adherence due to exported parasite proteins on the cell surface²⁵.

71 Here, we present a method to sort RBCs based on deformability and demonstrate the ability to
72 enrich ring stage *Pf*-iRBCs at clinically relevant concentrations to dramatically improve the sensitivity of
73 malaria diagnosis. Our method relies on ratchet transport created by deforming single cells through
74 tapered constrictions using oscillatory flow, enabling continuous and perpetual fractionation of the
75 input cell sample. The filtration microstructures remain unobstructed during the sorting process, which
76 ensures that all cells experience a consistent filtration force. Additionally, the oscillatory flow prevents
77 the adsorption of *Pf*-iRBCs to the filtration microstructure, enabling the extraction of target cells after
78 separation. We show this method can enrich ring-stage *Pf*-iRBCs by >100X, therefore dramatically
79 improving the detection limits of malaria diagnosis performed using microscopy and rapid diagnostic
80 tests (RDTs).

81 Our work here derives from our previous studies of the microfluidic ratchet mechanism where we
82 showed that 1) the force required to deform single cells through tapered constrictions are directionally
83 asymmetrical²⁶, 2) oscillatory deformation through such constrictions can produce a ratcheting
84 transport behavior that depends on cell deformability, and 3) the potential to use this effect to sort
85 nucleated cells based on deformability²⁷. Here, we extended these principles to RBCs, which are orders
86 of magnitude more deformable than nucleated cells^{28,29}. Furthermore, in our previous implementation²⁷,
87 the cell sample must be batch loaded into the microfluidic device using membrane micro-valves, which
88 limited the throughput to ~9000 cells per hour. Here, we developed a method to continuously sort RBCs
89 based on deformability that extended the sample throughput to ~0.5 million cells per hour, which is
90 sufficient to enrich for *Pf*-iRBCs at clinically relevant parasitemia.

Deformability based sorting of red blood cells



91
 92 **Figure 1. Design of the ratchet-sorting device.** (A-B) Tapered funnel constriction allowing unidirectional
 93 flow of cells under oscillation excitation which consists of (A) upward filtration flow and (B) downward
 94 de-clogging flow; (C) Cell sorting using a matrix of funnel constrictions. The cell sample is introduced
 95 through the sample inlet (SI) and forms a diagonal trajectory under the combined forces of cross-flow
 96 inlet (CFI) and biased-oscillation flows including oscillation inlet 1 (Osc1) for declogging and oscillation
 97 inlet 2 (Osc2) for filtration. More deformable cells, such as uiRBCs, will travel further up the matrix of
 98 funnel constrictions than less deformable cells, such as *Pf*-iRBCs, which will be blocked midway and be
 99 separated from the main population. (D) Image of microfluidic ratchet device infused with different
 100 food color dyes illustrating the diagonal trajectory of the SI through the ratchet-sorting device as well
 101 the nine outlets (O1-9) constituting a deformability gradient. (E) Image of the overview design of the
 102 ratchet sorting device.

103

104

Deformability based sorting of red blood cells

105 **RESULTS**106 **Deformability based Cell Sorting using Microfluidic Ratchets**

107 The principle of the microfluidic ratchet mechanism involves deforming single cells through tapered
108 constrictions significantly smaller than their diameter. The pressure required to deform the cell along
109 the direction of taper (**Figure 1A**) is less than the pressure required to deform the cell against the
110 direction of taper (**Figure 1B**)²⁶. Coupling this physical asymmetry with a biased oscillatory flow creates a
111 ratcheting effect that transports certain cells uni-directionally through the constriction while preventing
112 the transport of other cells. This transport process is selective on the basis of the cell's ability to squeeze
113 through a microscopic constriction, which simulates the transport and sequestration of RBCs in the
114 microvasculature. The oscillatory flow plays the critical role of minimizing contact between the cells and
115 the microstructures to prevent clogging and fouling in order to ensure that a consistent deformation
116 force is applied to each cell.

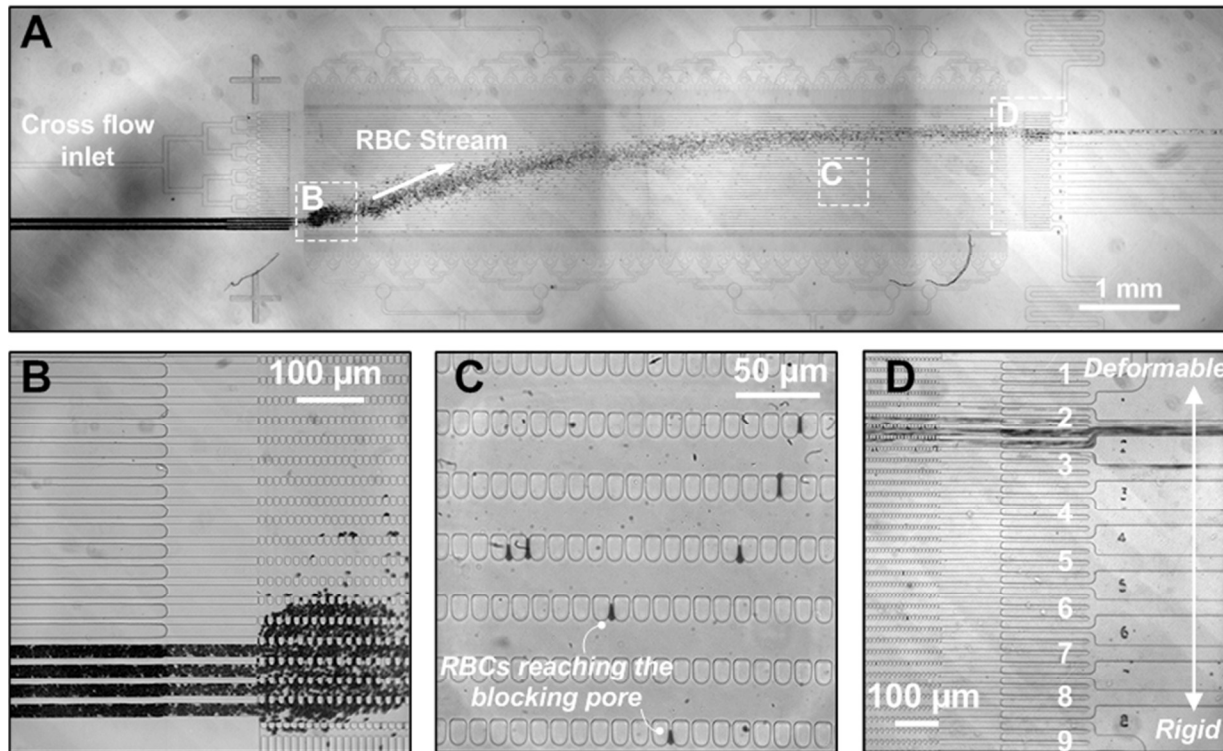
117 To sort RBCs using the microfluidic ratchet effect, a RBC sample is transported through a 2D array of
118 micrometer-scale tapered constrictions. The openings of the constrictions are gradually decreased from
119 the bottom row to the top row in order to test the ability of RBCs to transit through the constriction at
120 progressively smaller pores (**Figure 1C**). The cell sample is introduced at the bottom-left corner of the
121 array and transported through the array by a vertical oscillatory flow and a constant horizontal cross
122 flow. These flows combine to propel the cells in a zigzag diagonal path through the constriction matrix.
123 As cells reach their limiting constriction size where they are unable to transit, they proceed horizontally
124 between funnel rows towards the outlet. Since cells with different deformability will be restricted by
125 different constriction sizes, the cell population are sorted based on deformability in this manner
126 (**Figure 2**). A video of the sorting process is provided in the online supplementary materials.

127 **Microfluidic Device Design**

128 The constriction matrix used to sort RBCs consists of 35 rows and 630 columns of tapered
129 constrictions. The pore size is constant in each row, and decreases every four rows from bottom to the
130 top. In total, the 35 rows of constrictions consists of 9 different sizes (1.5, 1.75, 2, 2.25, 2.5, 3, 3.5, 6, and
131 7.5 μm), which sort the input sample based on deformability into 9 fractions in outlets O1-O9. The
132 thickness of the constriction matrix chamber is 4.5 μm , which is sufficient to constrain RBCs in a planar
133 configuration while still allowing them to be transported freely by fluid flow. Fluid flow in the
134 constriction matrix is controlled by fluid flow from supporting microchannels originating from the
135 sample inlet (SI), oscillation flow inlets (Osc1 and Osc2) and cross-flow inlet (CFI) (**Figure 1E**).

Deformability based sorting of red blood cells

136



137 **Figure 2. Micrographs of cell sorting using the microfluidic ratchets.** (A) RBCs follow a diagonal
 138 trajectory in response to the inlets flow, cross flow, and biased oscillatory flow (stitched image). (B) RBCs
 139 are introduced through the inlet, (C) transit the sorting matrix until reaching the blocking pore sizes,
 140 where (D) they proceed horizontally towards the appropriate outlet. The majority of the RBCs sample
 141 flow into the highly deformability fractions, while a minority rigid RBCs (such as *Pf*-iRBCs) are separated
 142 into the low deformability fractions.

143

144 **Hydrodynamic Model**

145 Fluid flow in a microfluidic channel is linearly proportional to the drop in pressure across the length
 146 of the channel. This linear proportionality, along with the required conservation of volume of
 147 incompressible flows, allows the analysis of fluid flow using standard methods of linear electrical circuit
 148 analysis. Specifically, the pressure and flow rate relationship can be determined from,

$$149 \quad \Delta P = R_H \times Q, \quad (1)$$

150 where ΔP is the pressure difference across a fluidic channel, Q is the volumetric flow rate, and R_H is the
 151 hydrodynamic resistance. The hydrodynamic circuit for the microfluidic device includes microchannels
 152 leading to the funnel matrix originating from the cross flow inlet (R_{CFI}), sample inlet (R_{SI}), oscillation (R_{OSC})
 153 and outlets (R_O) (**Supplemental Figure 1**). Fluid flow in funnel matrix can be considered as a

Deformability based sorting of red blood cells

154 superposition of the vertical oscillatory flow circuit and the horizontal constant flow circuit
 155 (**Supplemental Figure 2**). In the vertical circuit, the hydrodynamic resistance of the sorting matrix, $R_{SORT,V}$,
 156 can be determined by summing resistances of the individual funnel constrictions,

$$157 \quad R_{SORT,V} = \frac{\sum_i^{n_{row}} r_i}{n_{column}}, \quad (2)$$

158 where n_{row} and n_{column} are the number of funnel rows and columns in the matrix, r_i is the resistance of
 159 the individual funnel and the value of each r_i is determined using finite element simulation (COMSOL
 160 multiphysics, full listing of the values of r_i are in **Supplemental Table 1**). In the horizontal circuit, the
 161 hydrodynamic resistance of the sorting matrix, $R_{SORT,H}$, can be determined from the resistance of the
 162 spacing between each funnel row ($r_{spacing}$) using

$$163 \quad R_{SORT,H} = \frac{r_{spacing}}{n_{spacing}}, \quad (3)$$

164 where $n_{spacing}$ is the number of horizontal spacings in the sorting matrix.

165 The supporting microchannels are designed to present a dominant hydrodynamic resistance (>50X)
 166 over that of the funnel matrix, allowing precise control of fluid flow using pressure-driven flow from the
 167 inlets (full listing of the hydrodynamic resistance values are in **Supplemental Table 2**). This *heavy-*
 168 *peripheral-light-center* hydrodynamic design provides a constant flow rate in the funnel matrix, whose
 169 resistance may vary with the number of cells in the funnel matrix, and thereby ensures that each cell
 170 experiences a nearly constant deformation pressure. This design further serves to dramatically reduce
 171 the pressure applied at the inlets to derive an attenuated version for each cell. Specifically, the
 172 pressures ranging from 14 to 20 kPa applied at the oscillation inlets are reduced to less than 10 Pa at
 173 each funnel constriction, which we determined previously was appropriate to distinguish normal RBCs
 174 and ring-stage iRBC through similarly sized microfluidic constrictions^{28,30,31}.

175 **Microfluidic Device Operation**

176 Operation of the microfluidic device involves initially infusing the RBC population through the
 177 sample inlet and setting the pressures at the sample, oscillation, and cross flow inlets to produce a
 178 characteristic diagonal cell stream across the rectangular funnel array. The inlet pressure settings are
 179 determined empirically by observing the angle of the cell stream. If the oscillation pressure (Osc 2) is too

Deformability based sorting of red blood cells

180 low, the cell sample do not have sufficient time to test each row of funnel constrictions and will exit the
181 funnel array prematurely. If the oscillation pressure (Osc 2) is too high, the cells will exit the funnel array
182 at the upper boundary and then will not be transported to the outlets. The oscillatory cycle is set at 4
183 seconds upward followed by 1 second downward. The upward timing is selected to provide sufficient
184 time for each cell to test at least one funnel constriction per cycle, while the downward timing is
185 selected to provide sufficient time to release non-transiting cells from each constriction.

186 RBC Deformability Measurement

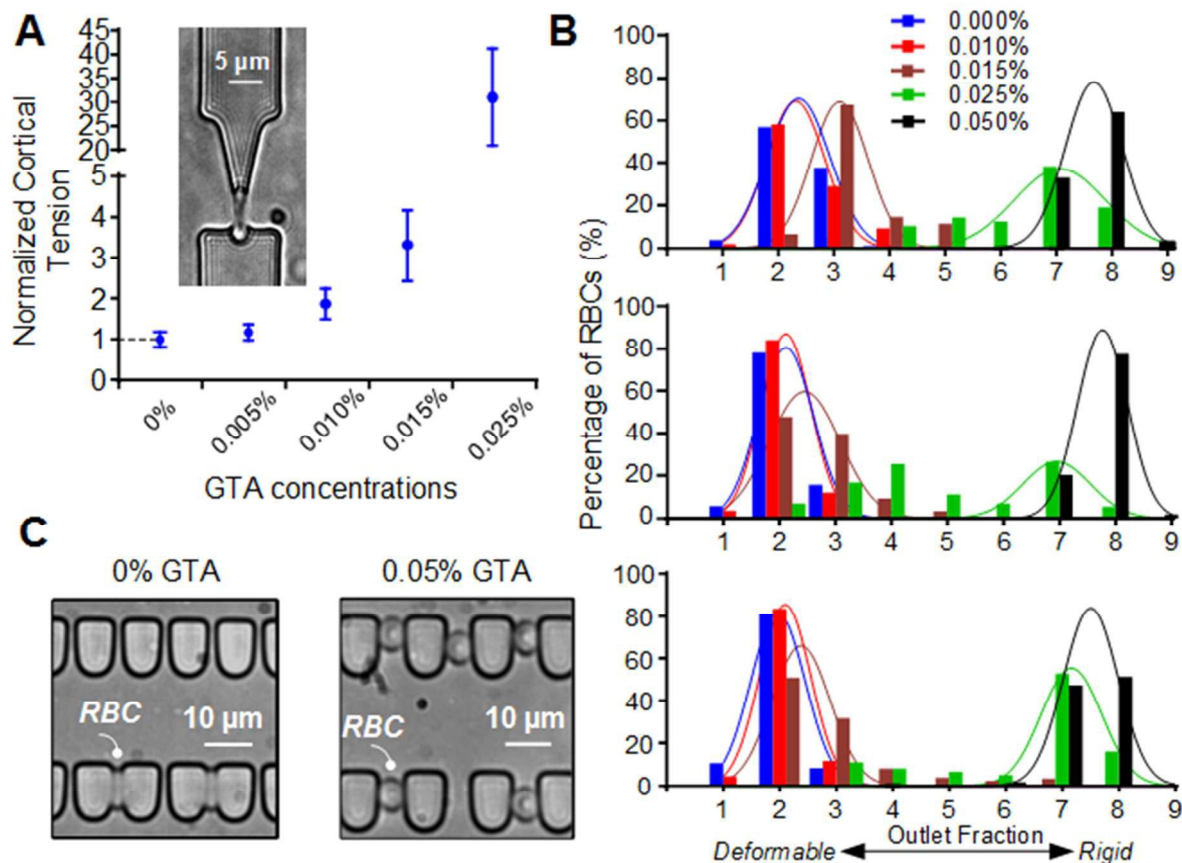
187 As preparation for deformability based sorting of RBCs, we first measured the deformability of RBCs
188 in the contexts relevant to this study. RBCs deformability has been previously measured using bulk flow
189 and single-cell approaches. Traditional bulk flow approaches, such as ektacytometry³²⁻³⁴ and filtration
190^{35,36}, provide the average deformability profile of a RBC population, but cannot discriminate properties in
191 minor subpopulation of the RBC sample, such as in RBCs infected with *P. falciparum*. This challenge has
192 motivated the development of single-cell deformability measurement techniques including optical
193 tweezer³⁷⁻³⁹, hydrodynamic flow^{40,41}, dielectrophoretic deformation force⁴², capillary obstruction⁴³,
194 membrane fluctuation⁴⁴, transit time through micrometer scale constrictions⁴⁵⁻⁴⁷, and transit pressure
195 through micrometer scale constrictions^{28,48}. Transit pressure through micrometer scale constrictions is
196 the approach most relevant to the current cell sorting work. Specifically, we used this approach to
197 measure the threshold pressure required to squeeze individual healthy RBCs, chemically degraded RBCs,
198 and *Pf*-iRBCs through constrictions size ranging from 2-5 μm , as shown in the inset image in **Figure 3A**.
199 The measured threshold deformation pressure is then converted to cortical tension using liquid drop
200 model to provide an intrinsic measure of deformability independent of constriction and RBC geometry.
201 Further details on this measurement technique are described in Guo *et al.* 2012²⁸ and Myrand-Lapierre
202 *et al.* 2014³¹.

203 Device Validation

204 To establish the ability of the ratchet mechanism to sort RBCs based on deformability, we
205 chemically degraded RBCs by exposing them to low concentrations of glutaraldehyde (GTA), a fixative
206 agent that induces cross-linking and stabilization of RBC membrane proteins to reduce deformability in a
207 concentration dependent manner. We verified this property by measuring the deformability (as defined
208 by their cortical tension) of normal RBCs exposed to 0.005% to 0.025% GTA (**Figure 3A**). GTA
209 concentrations greater than 0.025% will make RBCs entirely rigid and unable to be deformed through
210 the constriction at the maximum available pressure.

Deformability based sorting of red blood cells

211 We then sorted RBCs exposed to 0% to 0.05% GTA. The sorting process distributed these cells into
 212 the outlets in a manner consistent with their decreased deformability. Specifically, RBCs exposed to
 213 0.000% and 0.010% GTA were distributed in outlets 1 to 3, while increasing the GTA concentration to
 214 0.015%, 0.025%, and 0.05% resulted in progressive rightward shifts in their distribution (**Figure 3B**). RBCs
 215 exposed to 0.05% GTA retained their discoid shape even when deformed, which prevented them from
 216 transiting through 6 μm pores. This sorting experiment was repeated three times using RBCs from three
 217 different donors. The resulting RBC distributions were consistent and demonstrate the repeatability of
 218 the deformability based sorting process.



219

220 **Figure 3. Validation of deformability-based cell sorting using microfluidic ratchets.** (A) Comparison of
 221 deformability of RBCs rigidified by GTA at progressively increasing concentrations; (B) Normalized
 222 distributions across the outlets of the RBCs treated with various concentration of GTA for RBCs from
 223 three different donors. (C) Micrographs of 0% and 0.05% GTA treated RBCs in the funnel constrictions.

224

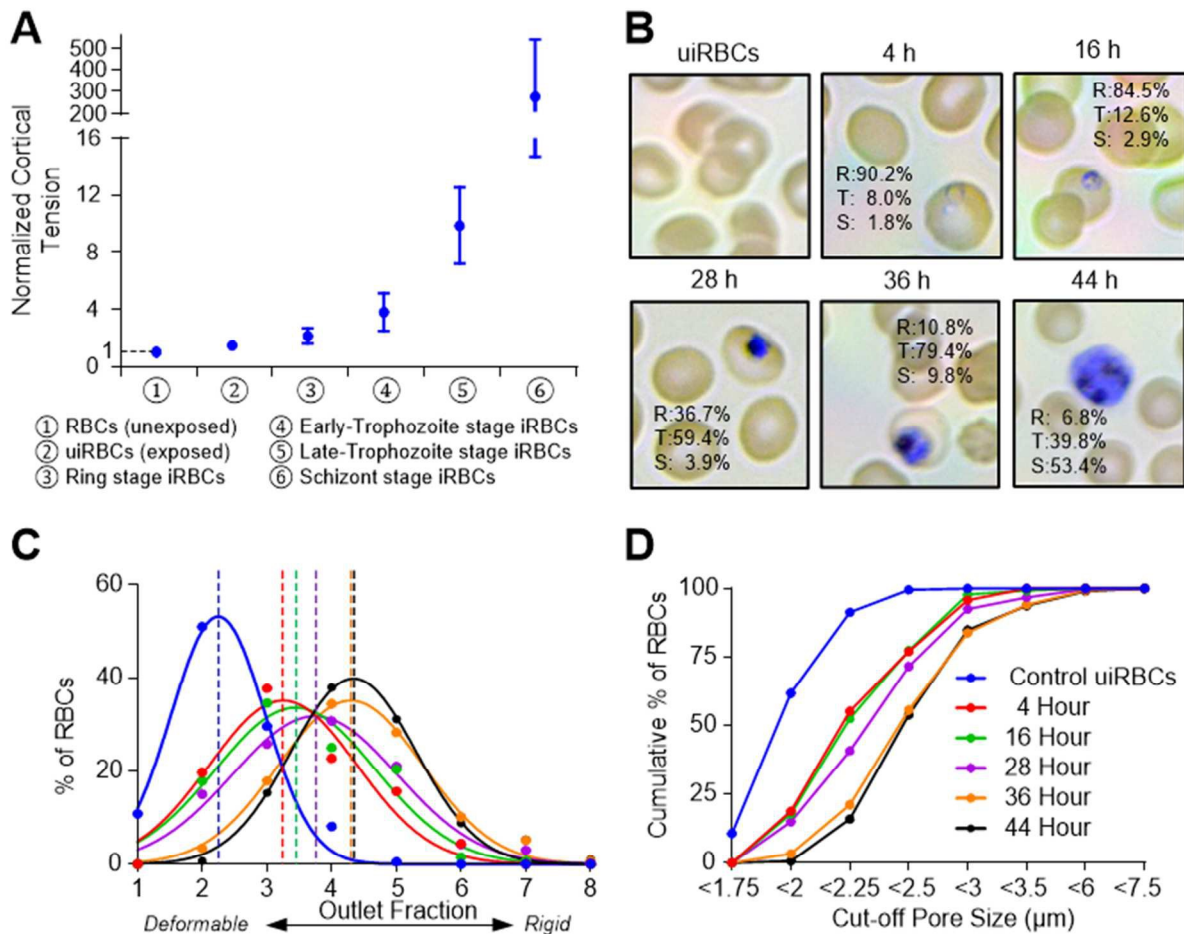
225

Deformability based sorting of red blood cells

226 **Deformability based Sorting of *Pf*-iRBCs**

227 The deformability of *Pf*-iRBCs at different intra-erythrocyte stages was measured previously to
228 provide an estimate of their distribution after sorting (**Figure 4A**)²⁸. We tested the potential to sort *Pf*-
229 iRBCs at different intra-erythrocyte stages of development using synchronized *Pf*-iRBCs (see Material
230 and Methods). Aliquots from a *P. falciparum* culture at 4, 16, 28, 36, 44 hours post-synchronization were
231 sorted and then counted (**Figure 4B**). Prior to processing, each sample is stained using Hoechst DNA
232 stain to facilitate enumeration of the *Pf*-iRBCs after sorting. Uninfected RBCs incubated in the identical
233 environment as the parasite culture were used as a control. These cells were primarily distributed in
234 outlets 1-4. At the 4 and 16 hour time points, *Pf*-iRBCs were predominantly at ring-stage and had a
235 distribution centered around outlet 3. At the 28, 36, and 44 hour time points, the *Pf*-iRBCs were
236 predominantly trophozoite and schizont stage, and had a distribution centered around outlets 4 and 5.
237 In general, the *Pf*-iRBC distribution exhibited a monotonic rightward shift directly correlated incubation
238 time after synchronization (**Figure 4C**), which can be better visualized as a cumulative distribution
239 (**Figure 4D**). The ability to distinguish *Pf*-iRBCs at different stages of development could likely be
240 improved by further optimization of the geometries of the constriction matrix (constriction width and
241 thickness), as well as the filtration pressure. Nonetheless, these results are consistent with our previous
242 efforts to measure the deformability of *Pf*-iRBCs at different stages of intra-erythrocyte development²⁸.

Deformability based sorting of red blood cells



243
 244 **Figure 4. Deformability-based sorting of *Pf*-iRBCs at different intra-erythrocyte stages.** (A) The
 245 deformability of freshly-drawn RBCs unexposed to parasite culture, exposed but uninfected RBCs
 246 (uiRBCs) from a *P. falciparum* culture, as well as *Pf*-iRBCs at the ring, early trophozoite, late trophozoite
 247 and schizont stages (from Guo *et al.* 2012²⁸). (B) Micrographs of Giemsa stained uiRBC and *Pf*-iRBCs at 4-
 248 44 hours post-synchronization. Percentages of iRBCs at ring (R), trophozoite (T) and schizont (S) stages at
 249 each time point are shown within the images. (C) Normalized distribution of uiRBCs and *Pf*-iRBCs at 4-44
 250 hours after ring-stage synchronization. (D) Result in C shown as cumulative distribution.

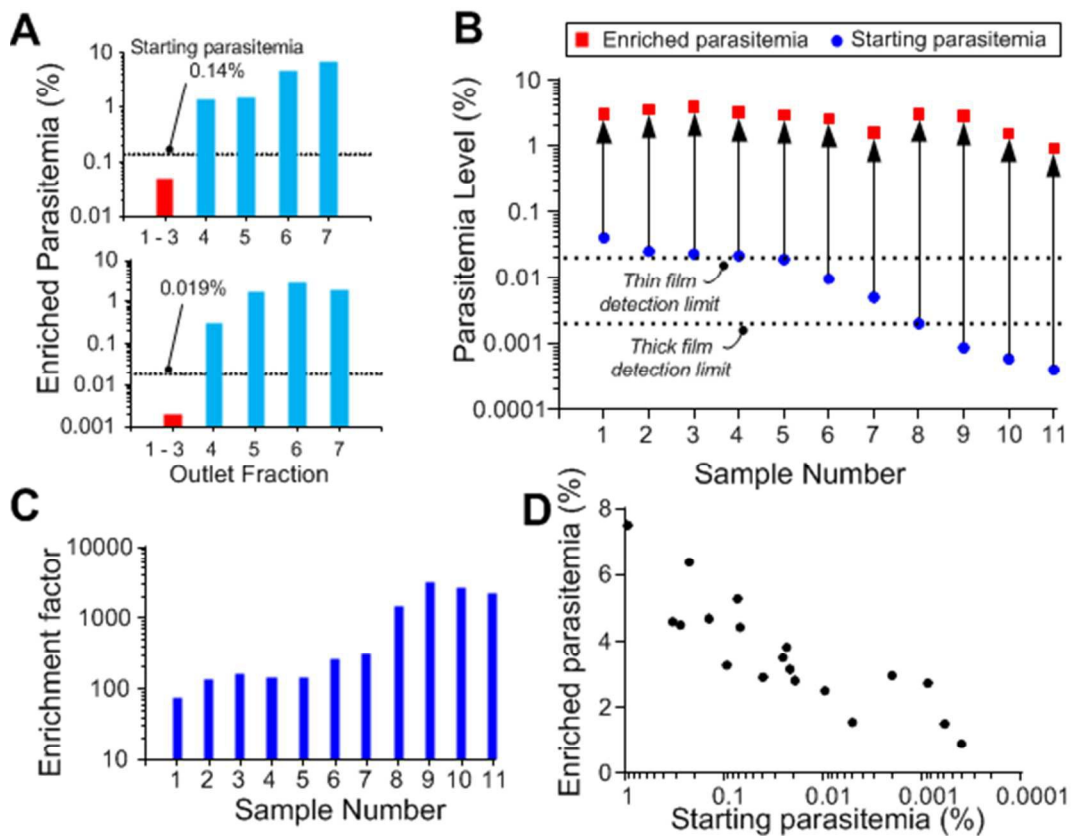
251 Improving the sensitivity of microscopy based malaria diagnosis

252 We studied the potential to use deformability based cell sorting to enrich for *Pf*-iRBCs to improve
 253 the sensitivity of malaria diagnosis performed using microscopy. To model clinical samples, *Pf*-iRBCs
 254 synchronized at the ring-stage with approximately 5% parasitemia were doped into uninfected RBCs to
 255 create the desired parasitemia. Initially, we sorted *Pf*-iRBCs samples at a moderately low parasitemia (0.01%-
 256 0.1%) in order to determine the outlets distribution of *Pf*-iRBCs. *Pf*-iRBCs were significantly enriched in
 257 outlets 4-7 and depleted in outlets 1-3 (Figure 5A).

258 To investigate the enrichment of ring-stage *Pf*-iRBCs at low parasitemia, a series of samples with
 259 parasitemia ranging from 0.04% to 0.0004% were prepared and sorted. Fractionated samples collected

Deformability based sorting of red blood cells

260 from outlets 4-7 were pooled together to measure the resulting parasitemia. Samples with starting
 261 parasitemia orders of magnitude lower than the detection limits of thin-film and thick-film microscopy
 262 were enriched to a detectable range (1-3% parasitemia, **Figure 5B**), equivalent to enrichment factors of
 263 100X to 2500X (**Figure 5C**). The uninfected RBCs sorted into outlets 4-7 are likely to be RBCs that
 264 experience a loss of deformability resulting from natural aging and senescence⁴⁹⁻⁵¹, as well as from
 265 exposure to heme by-products released from *Pf*-iRBCs⁵. The latter effect is likely responsible for the
 266 observed relationship between enrichment and initial parasitemia, where the sorting process provides
 267 greater enrichment for samples with lower initial parasitemia (**Figure 5D**). Regardless of these effects,
 268 however, our results show that deformability-based ratchet sorting is able to dramatically lower the
 269 detection limit of malaria diagnosis performed using microscopy.



270
 271

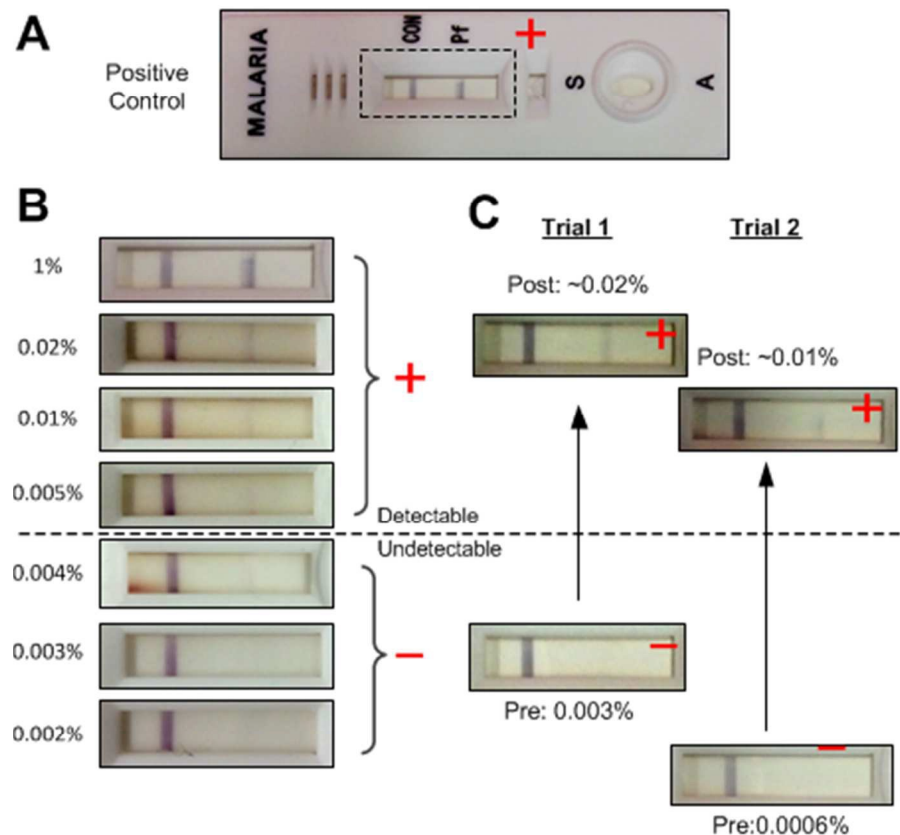
272 **Figure 5. Deformability based sorting of RBCs improves the sensitivity of malaria diagnosis performed**
 273 **using microscopy.** (A) The distribution of *Pf*-iRBCs in low-parasitemia samples after sorting by the
 274 microfluidic ratchet. *Pf*-iRBCs selectively accumulate in outlets 4-7 and can achieve an increasingly
 275 greater magnitude of enrichment for samples with a low starting parasitemia (indicated by dotted line).
 276 (B) Enrichment of *Pf*-iRBC from 11 samples with parasitemia ranging from 0.04% to 0.0004%. The output
 277 sample was pooled from outlets 4-7. The initial and enriched parasitemia is shown relative to the
 278 detection limit for thin and thick film microscopy. (C) The resulting enrichment factors from the 11

Deformability based sorting of red blood cells

279 samples. (D) Dot plot showing the correlation between the initial parasitemia and the enriched
280 parasitemia.

281 Improving the sensitivity of rapid diagnostic tests

282 Finally, we investigated the potential to use deformability based cell sorting to improve the
283 sensitivity of malaria diagnosis performed using rapid diagnostic tests (RDT). RDT strips based on
284 plasmodium lactate dehydrogenase (pLDH) were selected because of their low false positive rate⁵². We
285 evaluated RDT sensitivity over a range of parasitemia and established their detection limit to be 0.004%
286 parasitemia (**Figure 6B**). We then prepared ring-stage *Pf*-iRBC samples at 0.003% and 0.0006%
287 parasitemia, as well as a positive control at 0.1% parasitemia. The RDT was not able to detect the
288 infection without enrichment, whereas the enriched output pooled from outlets 4-7 of the microfluidic
289 device were detected. In these cases, the optical density of the detection band for the enriched samples
290 were similar to 0.02% or 0.01% parasitemia respectively (**Figure 6C**). These results confirm that
291 microfluidic enrichment could dramatically increase the sensitivity of RDTs for *falciparum* malaria.



292

293 **Figure 6. Deformability based sorting of RBCs improves the sensitivity of malaria diagnosis performed**
294 **using RDTs.** (A) Example of malaria RDT indicating a positive result. (B) Titration of RDT result as a
295 function of parasitemia showing the indicator band become undetectable at $<0.005\%$ parasitemia. (C)

Deformability based sorting of red blood cells

296 Following microfluidic enrichment of parasitized cells, samples with undetectable parasitemia (0.003%
297 and 0.0006%) were enriched to detectable parasitemia (estimated as 0.02% and 0.01% respectively).

298

299 DISCUSSION

300 Reduced RBC deformability is central to the pathology of *falciparum* malaria. Consequently,
301 deformability based sorting represents a fundamental approach that could be used to enrich for
302 pathological cells to improve diagnostic sensitivity or to fractionate these cells for further study.
303 However, deformability based sorting of RBCs has not been previously achieved because of the extreme
304 softness of these cells, which requires exquisite control of the deformation force applied to each cell in
305 order to alter its flow path. The microfluidic ratchet mechanism provides a means to continuously filter
306 sample cells without allowing them to arrest and accumulate in the filtration microstructure. This
307 approach ensures that a consistent filtration force is applied to each cell, enabling highly selective
308 sorting without immobilizing cells on the filter.

309 Deformability-based sorting could overcome a key challenge associated with the detection of
310 malaria infection at low parasitemia in early stage infection and asymptomatic individuals. While
311 existing high-sensitivity malaria detection methods involve PCR-based analyses⁵³ that require specialized
312 laboratory infrastructure, the ability to biophysically enrich for infected RBCs by 100X (and potentially
313 up to 2500X) could effectively lower the limit of detection for malaria diagnosis performed using
314 conventional microscopy and RDT methods. Furthermore, microfluidic enrichment could be used to
315 develop simple diagnosis platforms based on automated microscopy^{54,55}, where existing methods are
316 currently limited by error rate and throughput.

317 Finally, since change in iRBC deformability is directly correlated with parasite development and
318 maturation, successful fractionation of *Pf*-iRBCs at various development stages could potentially aid the
319 discovery of biomarkers associated with parasite growth and drug metabolism through RNA sequencing
320 and proteomics. In addition to malaria, this approach could potentially be used to discover the
321 underlying molecular mechanisms in sickle cell disease⁵⁶ and RBC senescence⁵⁷ where RBC deformability
322 is thought to play a central role.

323

Deformability based sorting of red blood cells

324 **MATERIAL AND METHODS**325 **Microfluidic fabrication**

326 **Photolithography.** The microfluidic ratchet device consists of a single fluidic layer fabricated using
327 soft-lithography of polydimethylsiloxane (PDMS) silicone. Mold for the microstructure consists of two
328 photo-lithographically defined layers fabricated on a silicon wafer. The funnel matrix was fabricated
329 using SU-8 3005 photoresist (MicroChem, Newton, MA, USA) thinned with cyclopentanone at a ratio of
330 1:0.8 by volume. The supporting microfluidic channels were made from SU-8 3010 photoresist. The
331 patterns for both masks were drawn using Solidworks DWG Editor.

332 The SU-8 3005 microstructures were fabricated on a cleaned 100 mm silicon wafer. After
333 dehydration baking on a hotplate at 200°C for 5 minutes, thinned SU-8 3005 was spread onto the wafer
334 at 500 rpm for 10 seconds, and then spun at 4000 rpm for 30 seconds to remove the edge beads. The
335 wafer was then soft baked at 95°C on the hot plate for 20 minutes before being exposed to UV light in a
336 mask aligner for 30 seconds. The exposed wafer was given a post exposure bake in the sequence of 65°C
337 for 1 minute, 95°C for 1.5 minute and then 65°C for 1 minute. The wafer was then developed using SU-8
338 developer (MicroChem). The geometry of the SU-8 3005 photoresist was stabilized by further baking on
339 a hotplate where the temperature was gradually ramped from 40°C to 200°C, held at 200°C for one hour,
340 and then gradually cooled to 40°C. The finished SU-8 structure was measured to be 4.5 μm in thickness
341 using profilometer (Alpha step 200).

342 The SU-8 3010 microstructures were added to the silicon wafer containing the SU-8 3005
343 microstructures. SU-8 3010 photoresist was spin-coated on the wafer at 3000 rpm for 50 seconds, and
344 then at 4000 rpm for 2 seconds. The coated wafer was soft baked on hotplates set at 65°C for 1 minute,
345 95°C for 2 minutes, and then 65°C for 1 minute. The designed mask for the SU-8 3010 pattern was then
346 aligned with the SU-8 3005 pattern and exposed for 4 minutes in 30 seconds bursts. After waiting for
347 approximately 30 minutes, the wafer was developed using SU-8 developer (MicroChem). The finished
348 structure was measured to be 10 μm in thickness using profilometer (Alpha Step 200).

349 **Soft-lithography.** Replicas of the silicon wafer molds were fabricated using a polyurethane-based
350 plastic (Smooth-Cast ONYX SLOW, Smooth-On) using the process described by Desai⁵⁸. PDMS
351 microfluidic devices were then fabricated from these molds using soft-lithography of RTV 615 PDMS
352 (Momentive Performance Materials).

Deformability based sorting of red blood cells

353 After baking, the cured microfluidic device was removed from its mold, and holes were punched into
354 it using a 0.5 mm outer diameter hole punch (Technical Innovations, Angleton, TX, USA) as the fluidic
355 introduction ports including cross flow and cell inlets as well as the oscillation inlets. The outlets are
356 punched using 4 mm diameter puncher. The microfluidic device is then bonded to a blank layer of PDMS
357 spin-coated onto a blank silicon wafer at 1500 rpm for 1 minutes. The device containing a blank layer of
358 PDMS at bottom is then peeled off. The bonding is realized through the exposure of both surfaces to
359 oxygen plasma (Model PDC-001, Harrick Plasma) for 70 seconds before the PDMS device is brought into
360 contact with the blank PDMS layer to create a permanent covalent bond. After peeled off from the
361 wafer, the double layer device is subsequently bonded to the standard microscope slide (Fisher
362 Scientific) cleaned beforehand with acetone and isopropanol.

363 Blood preparation

364 **Normal Packed RBCs.** Blood from healthy donors was obtained via venipuncture in tube containing
365 EDTA anti-coagulant, following informed consent and approval from the University of British Columbia
366 (UBC) Research Ethics Board. The whole blood was spun down at 3000 g for 10 minutes. The plasma, the
367 buffy coat and the top layer of the cells were then removed. The remaining cells are normal packed
368 RBCs. For the glutaraldehyde study, the packed RBCs were used within the same day. Packed RBCs were
369 also used to feed the *Plasmodium falciparum* parasites.

370 **Glutaraldehyde Treatment.** Packed RBCs were suspended in Phosphate Buffered Saline (PBS; CaCl₂-
371 free and MgSO₄-free; Invitrogen) with 0.2% Pluronic™ F-127 (Invitrogen). Diluted RBCs were incubated
372 for 30 minutes at 25°C with 0 to 0.05% glutaraldehyde (GTA; Alfa Aesar, MA). After incubation, the RBCs
373 suspension was washed three times in PBS and then re-suspended in PBS with 0.2% Pluronic.

374 ***P. falciparum* Culture and Ring Stage Synchronization.** The 3D7 strain of *P. falciparum* parasites was
375 cultured under standard *in vitro* conditions with modifications⁵⁹. Type A+ blood was collected from
376 healthy donors with written informed consent and approval from the Research Ethics Boards of UBC and
377 Canadian Blood Services (CBS) by the CBS' Network Centre of Applied Development. Cultures were
378 maintained at approximately 5% hematocrit in malaria culture medium (1640 RPMI with HEPES; 0.2%
379 sodium bicarbonate; 100 μM hypoxanthine; 10% heat-inactivated human serum; 1 mg/ml gentamicin).
380 Parasites were incubated in an atmosphere of 5% CO₂, 3% O₂ and 92% N₂ at 37°C and 95% humidity. To
381 achieve synchronous *falciparum* culture, 5% (w/v) sorbitol solution was dissolved thoroughly in distilled
382 water and warmed at 37°C for 5 minutes. Malaria culture at 50% was added to the sorbitol solution at
383 1:9 ratio. The mixture was incubated for 8 minutes at 37°C following 30 seconds of vigorous vortex to

Deformability based sorting of red blood cells

384 rupture old and mature parasites. Then centrifuge the sample at 250 g for 5 minutes at 37°C and remove
385 the supernatant. The synchronous culture with mostly ring parasites was cleaned twice with culture
386 medium at 250 g for 5 minutes.

387 **Magnetic Column Purification.** Magnetic column purification was used in conjunction with sorbitol
388 treatment to achieve tighter synchronous sample. A magnetic purification stand was fabricated based
389 on the design by Charles C. Kim⁶⁰ with some modifications to fit super magnets. LS columns (Miltenyi
390 Biotec, Bergisch Gladbach, Germany) which are designed for positive selection of strongly magnetically
391 labeled cells were used. They were initially washed once with 5 ml incomplete RPMI medium (10.4 g/l
392 RPMI-1640, 25 mM HEPES, 0.5% AlbuMAX I (w/v), 100 µM hypoxanthine, 12.5 µg/ml gentamicin) before
393 loading sorbitol synchronized sample (2% hematocrit). The subpopulation trapped by the magnet was
394 discarded while the eluted sample was transferred into a 15 ml Falcon tube (Corning Life Science,
395 Tewksbury, MA, USA), which was washed twice by centrifuging at 2000 rpm for 5 minutes without brake.

396 **Parasite Staining Processes**

397 **Giemsa Staining.** Blood smears of the cell cultures of approximately 50% hematocrit (asynchronous
398 and synchronous) were prepared onto a slide. The specimens were air-dried, fixed in methanol and
399 stained with 10% Giemsa to evaluate the stages of the infected RBCs. Parasitemia was determined by
400 counting at least 1000 RBCs under regular light microscope, equipped with a 100X oil-immersion
401 objective. Microscopic pictures were taken with Nikon camera mounted on the microscope. Images of
402 the Giemsa stained *Pf*-iRBCs were shown in **Supplemental Figure 3A**.

403 **Hoechst Fluorescence Staining.** Synchronous sample was stained with Hoechst 33342 (sigma)
404 before introduced through the device. Hoechst (5 µg/ml) were added to the sample at roughly 20%
405 hematocrit at 1:100 (v/v) in PBS solution with 2% heat-inactivated fetal bovine serum (FBS). The stained
406 *falciparum* sample were incubated for 20 minutes in room temperature in the dark. The sample, after
407 sorting, was observed under fluorescence microscope and images of stained *Pf*-iRBCs are shown in
408 **Supplemental Figure 3B**.

409 **Rapid Diagnostic Tests (RDTs)**

410 Rapid diagnostic tests detect malaria infection based on the presence of parasite specific antigens,
411 which produces a color change on an absorbent test strip. The two primary antigens used to detect
412 *falciparum* malaria are *Plasmodium falciparum* histidine-rich protein 2 (*Pf*HRP2) and *Plasmodium* lactate
413 dehydrogenase (pLDH). *Pf*HRP2 is believed to be more sensitive but suffers from false-positives due to

Deformability based sorting of red blood cells

414 antigen persistence following parasite clearance. RDTs based on pLDH do not suffer from antigen
415 persistence but are less sensitive than PfHRP2-based RDTs^{61,62}. For the RDT tests, CareStart™ test strips
416 for pLDH antigen were purchased from AccessBIO. Malaria samples containing low density ring stage *Pf*-
417 iRBCs were tested before and after the microfluidic enrichment. Pre-sorting samples were prepared at
418 40% hematocrit and a 5 μ l aliquot was transferred into the RDT reservoir for testing. Post-sorting
419 samples were prepared by pooling samples from outlets 4-9 together, and then centrifuged to remove
420 the excess supernatant. The remaining cells, suspended in 5 μ l of liquid, are then transferred into the
421 reservoir of the RDT for testing.

422

423

Deformability based sorting of red blood cells

424 REFERENCES

- 425 1 H. A. Cranston, C. W. Boylan, G. L. Carroll, S. P. Suter, J. R. Williamson, I. Y. Gluzman, D. J. Krogstad,
426 R. Williamson, I. Y. Gluzman and D. J. Krogstad, *Science*, 1984, **223**, 400–403.
- 427 2 M. Paulitschke and G. B. Nash, *J. Lab. Clin. Med.*, 1993, **122**, 581–589.
- 428 3 G. B. Nash, C. S. Johnson, H. J. Meiselman, B. Nash and C. S. Johnson, *Blood*, 1984, **63**, 73–82.
- 429 4 S. L. Schrier, *Annu. Rev. Med.*, 1994, **45**, 211–218.
- 430 5 F. Nuchsongsin, K. Chotivanich, P. Charunwatthana, O.-S. Fausta, D. Taramelli, N. P. Day, N. J. White
431 and A. M. Dondorp, *Am J Trop Med Hyg*, 2007, **77**, 617–622.
- 432 6 E. M. Rivadeneira, M. Wasserman and C. T. Espinal, *J. Protozool.*, 1983, **30**, 367–370.
- 433 7 S. Philipp, H.-H. Oberg, O. Janssen, M. Leippe and C. Gelhaus, *Cytometry. A*, 2012, **81**, 1048–1054.
- 434 8 G. Jun, J.-S. Lee, Y.-J. Jung and J.-W. Park, *J. Korean Med. Sci.*, 2012, **27**, 1137–1142.
- 435 9 D. Holmes, G. Whyte, J. Bailey, N. Vergara-Irigaray, a. Ekpenyong, J. Guck and T. Duke, *Interface*
436 *Focus*, 2014, **4**, 20140011–20140011.
- 437 10 T. Krueger, D. Holmes and P. Coveney, *Biomicrofluidics*, 2014, **8**, 1–10.
- 438 11 H. W. Hou, A. A. S. Bhagat, A. G. L. Chong, P. Mao, K. S. W. Tan, J. Han and C. T. Lim, *Lab Chip*, 2010,
439 **10**, 2605–2613.
- 440 12 T. M. Geislinger, S. Chan, K. Moll, A. Wixforth, M. Wahlgren and T. Franke, *Malar. J.*, 2014, **13**, 375.
- 441 13 S. Choi, J.-K. Park, P. Gascoyne, C. Mahidol, M. Ruchirawat, J. Satayavivad, P. Watcharasit and F. F.
442 Becker, *Lab Chip*, 2002, **2**, 70–75.
- 443 14 Y.-H. Hsu, P. Lu, J. L. Coleman and W. C. Tang, *Biomed. Microdevices*, 2011, **13**, 995–1004.
- 444 15 I. Safeukui, J.-M. Correas, V. Brousse, D. Hirt, G. Deplaine, S. Mulé, M. Lesurtel, N. Goasguen, A.
445 Sauvanet, A. Couvelard, S. Kerneis, H. Khun, I. Vigan-Womas, C. Ottone, T. J. Molina, J.-M. Tréluyer,
446 O. Mercereau-Puijalon, G. Milon, P. H. David and P. A. Buffet, *Blood*, 2008, **112**, 2520–2528.
- 447 16 A. M. Dondorp, P. A. Kager, J. Vreeken and N. J. White, *Parasitol. Today*, 2000, **16**, 228–232.
- 448 17 F. Paul, S. Roath, D. Melville, D. C. Warhurst and J. O. S. Osisanya, *Lancet*, 1981, **318**, 70–71.
- 449 18 J. Nam, H. Huang, H. Lim, C. Lim and S. Shin, *Anal. Chem.*, 2013, **85**, 7316–7323.
- 450 19 S. Zheng, H. Lin, J.-Q. Liu, M. Balic, R. Datar, R. J. Cote and Y.-C. Tai, *J. Chromatogr. A*, 2007, **1162**,
451 154–61.
- 452 20 I. Desitter, B. S. Guerrouahen, N. Benali-Furet, J. Wechsler, P. A. Jänne, Y. Kuang, M. Yanagita, L.
453 Wang, J. A. Berkowitz, R. J. Distel and Y. E. Cayre, *Anticancer Res.*, 2011, **31**, 427–441.
- 454 21 G. Vona, A. Sabile, M. Louha, V. Sitruk, S. Romana, K. Schütze, F. Capron, D. Franco, M. Pazzagli, M.
455 Vekemans, B. Lacour, C. Bréchet and P. Paterlini-Bréchet, *Am. J. Pathol.*, 2000, **156**, 57–63.
- 456 22 X. Qin, S. Park, S. P. Duffy, K. Matthews, R. R. Ang, T. Todenhöfer, H. Abdi, A. Azad, J. Bazov, K. N. Chi,
457 P. C. Black and H. Ma, *Lab Chip*, 2015, **15**, 2278–2286.
- 458 23 H. M. Ji, V. Samper, Y. Chen, C. K. Heng, T. M. Lim and L. Yobas, *Biomed. Microdevices*, 2008, **10**,
459 251–257.
- 460 24 V. VanDelinder and A. Groisman, *Anal. Chem.*, 2007, **79**, 2023–2030.
- 461 25 C. A. Moxon, G. E. Grau and A. G. Craig, *Br. J. Haematol.*, 2011, **154**, 670–679.
- 462 26 Q. Guo, S. McFaul and H. Ma, *Phys. Rev. E*, 2011, **83**, 051910.
- 463 27 S. M. McFaul, B. K. Lin and H. Ma, *Lab Chip*, 2012, **12**, 2369–76.
- 464 28 Q. Guo, S. J. Reiling, P. Rohrbach and H. Ma, *Lab Chip*, 2012, **12**, 1143–50.
- 465 29 Q. Guo, S. Park and H. Ma, *Lab Chip*, 2012, **12**, 2687–95.
- 466 30 A. T. Santoso, X. Deng, J.-H. Lee, K. Matthews, S. P. Duffy, E. Islamzada, S. M. McFaul, M.-E. Myrand-
467 Lapiere and H. Ma, *Lab Chip*, 2015, **15**, 4451–4460.
- 468 31 M.-E. Myrand-Lapiere, X. Deng, R. R. Ang, K. Matthews, A. T. Santoso and H. Ma, *Lab Chip*, 2014, **15**,
469 159–167.

Deformability based sorting of red blood cells

- 470 32 W. Groner, N. Mohandas and M. Bessis, *Clin. Chem.*, 1980, **26**, 1435–1442.
471 33 S. Shin, Y. Ku, M.-S. Park and J.-S. Suh, *Cytometry B. Clin. Cytom.*, 2005, **65**, 6–13.
472 34 O. K. Baskurt, M. R. Hardeman, M. Uyuklu, P. Ulker, M. Cengiz, N. Nemeth, S. Shin, T. Alexy and H. J.
473 Meiselman, *Biorheology*, 2009, **46**, 251–64.
474 35 H. L. Reid, A. J. Barnes, P. J. Lock, J. A. Dormandy and T. L. Dormandy, *J. Clin. Pathol.*, 1976, **29**, 855–
475 8.
476 36 J. Stuart, *J. Clin. Pathol.*, 1985, **38**, 965–77.
477 37 M. Dao, C. T. Lim and S. Suresh, *J. Mech. Phys. Solids*, 2003, **51**, 2259–2280.
478 38 K. Bambardekar, A. K. Dharmadhikari, J. a Dharmadhikari, D. Mathur and S. Sharma, *J. Biomed. Opt.*,
479 2014, **13**, 064021.
480 39 G. Lenormand and A. Richert, *Biophys. J.*, 1999, **76**, 1145–1151.
481 40 S. Cha, T. Shin, S. S. Lee, W. Shim, G. Lee, S. J. Lee, Y. Kim and J. M. Kim, *Anal. Chem.*, 2012, **84**,
482 10471–7.
483 41 D. R. Gossett, H. T. K. Tse, S. A. Lee, Y. Ying, A. G. Lindgren, O. O. Yang, J. Rao, A. T. Clark and D. Di
484 Carlo, *Proc. Natl. Acad. Sci. U. S. A.*, 2012, **109**, 7630–5.
485 42 I. Doh, W. Lee, Y. Cho, A. Pisano and F. Kuypers, *16th Int. Conf. Miniaturized Syst. Chem. Life Sci.*,
486 2012, **173702**, 242–244.
487 43 J. P. Shelby, J. White, K. Ganesan, P. K. Rathod and D. T. Chiu, *Proc. Natl. Acad. Sci. U. S. A.*, 2003,
488 **100**, 14618–14622.
489 44 Y. Park, M. Diez-Silva, G. Popescu, G. Lykotrafitis, W. Choi, M. S. Feld and S. Suresh, *Proc. Natl. Acad.*
490 *Sci. U. S. A.*, 2008, **105**, 13730–13735.
491 45 S. Huang, A. Undisz, M. Diez-Silva, H. Bow, M. Dao and J. Han, *Integr. Biol. (Camb.)*, 2013, **5**, 414–22.
492 46 Y. Zheng, E. Shojaei-Baghini, A. Azad, C. Wang and Y. Sun, *Lab Chip*, 2012, **12**, 2560.
493 47 A. Adamo, A. Sharei, L. Adamo, B. Lee, S. Mao and K. F. Jensen, *Anal. Chem.*, 2012, **84**, 6438–6443.
494 48 Q. Guo, S. P. Duffy, K. Matthews, A. T. Santoso, M. D. Scott and H. Ma, *J. Biomech.*, 2014, **47**, 1767–
495 76.
496 49 K. Matthews, M.-E. Myrand-Lapierre, R. R. Ang, S. P. Duffy, M. D. Scott and H. Ma, *J. Biomech.*, 2015.
497 50 F. H. Bosch, J. M. Werre, L. Schipper, B. Roerdinkholder-Stoelwinder, T. Huls, F. L. Willekens, G.
498 Wichers and M. R. Halie, *Eur. J. Haematol.*, 1994, **52**, 35–41.
499 51 S. P. Sutera, R. A. Gardner, C. W. Boylan, G. L. Carroll, K. C. Chang, J. S. Marvel, C. Kilo, B. Gonen and
500 J. R. Williamson, *Blood*, 1985, **65**, 275–82.
501 52 J. Maltha, I. Guiraud, P. Lompo, B. Kaboré, P. Gillet, C. Van Geet, H. Tinto and J. Jacobs, *Malar. J.*,
502 2014, **13**, 20.
503 53 N. Tangpukdee, C. Duangdee, P. Wilairatana and S. Krudsood, *Korean J. Parasitol.*, 2009, **47**, 93–102.
504 54 Y. Purwar, S. L. Shah, G. Clarke, A. Almugairi and A. Muehlenbachs, *Malar. J.*, 2011, **10**, 364.
505 55 M. Sheikhhosseini, H. Rabbani, M. Zekri and A. Talebi, *J. Microsc.*, 2013, **252**, 189–203.
506 56 M. R. Clark, N. Mohandas and S. B. Shohet, *J. Clin. Invest.*, 1980, **65**, 189–96.
507 57 F. H. Bosch, J. M. Werre, B. Roerdinkholder-Stoelwinder, T. H. Huls, F. L. Willekens and M. R. Halie,
508 *Blood*, 1992, **79**, 254–260.
509 58 S. P. Desai, D. M. Freeman and J. Voldman, *Lab Chip*, 2009, **9**, 1631–7.
510 59 W. Trager and J. B. Jensen, *Science*, 1976, **193**, 673–5.
511 60 C. C. Kim, E. B. Wilson and J. L. DeRisi, *Malar. J.*, 2010, **9**, 17.
512 61 J. C. Mouatcho and J. P. Dean Goldring, *J. Med. Microbiol.*, 2013, **62**, 1491–1505.
513 62 A. Moody, *Clin. Microbiol. Rev.*, 2002, **15**, 66–78.
514